

# Study of a novel ALD process for depositing MgF<sub>2</sub> thin films

Tero Pilvi,<sup>\*a</sup> Timo Hatanpää,<sup>a</sup> Esa Puukilainen,<sup>a</sup> Kai Arstila,<sup>†b</sup> Martin Bischoff,<sup>c</sup> Ute Kaiser,<sup>d</sup> Norbert Kaiser,<sup>e</sup> Markku Leskelä<sup>a</sup> and Mikko Ritala<sup>a</sup>

Received 16th July 2007, Accepted 19th October 2007

First published as an Advance Article on the web 31st October 2007

DOI: 10.1039/b710903b

Magnesium fluoride is an ultraviolet (UV) transparent material which is widely used in optical applications over a wide wavelength range. We have developed a novel atomic layer deposition (ALD) process for depositing magnesium fluoride thin films for the first time. MgF<sub>2</sub> films were grown at 250–400 °C using Mg(thd)<sub>2</sub> and TiF<sub>4</sub> as precursors. The crystallinity, morphology, composition, thicknesses and refractive indices of the films were analyzed by X-ray diffraction/reflection (XRD/XRR), transmission electron microscopy (TEM), atomic force microscopy (AFM), field emission scanning electron microscopy (FESEM), time-of-flight elastic recoil detection analysis (TOF-ERDA), and UV-vis spectrophotometry. Electrical properties were also measured. The growth rate was temperature dependent decreasing from 1.6 Å cycle<sup>-1</sup> at 250 °C to 0.7 Å cycle<sup>-1</sup> at 400 °C. The films were polycrystalline at 250–400 °C. The refractive indices were between 1.34–1.42 and the permittivity 4.9. The impurity levels were below 0.6 at.% in the films deposited at 350–400 °C.

## Introduction

The push for higher density semiconductor devices requires smaller circuit features.<sup>1</sup> These can only be obtained by reducing the wavelength in the photolithographic process used to create the circuits. Line widths decrease in proportion to the wavelength of the light used in exposing the features. Optical components and their coatings are being forced to operate at wavelengths in the deep ultraviolet (UV) region. UV materials have applications also in fluorescence diagnostics, high energy astronomy and physics, and gas species detection, to name a few. Highly damage-resistant dielectric optical coatings are also essential for high output UV lasers.

Magnesium fluoride thin film is a promising UV transparent material like other large band gap fluorides (*e.g.* LaF<sub>3</sub>) and oxides (*e.g.* Al<sub>2</sub>O<sub>3</sub>). Bulk MgF<sub>2</sub> is a large band gap (about 12.8 eV) material having the rutile crystal structure.<sup>2</sup> It is also hard, has good stability in hostile environments and a low refractive index of 1.38.<sup>3</sup> MgF<sub>2</sub> thin films are suited for deep UV laser optics because no intrinsic material properties have been identified which might limit the laser durability of MgF<sub>2</sub> thin films at low fluences.<sup>4</sup> It has also been reported that dielectric losses of MgF<sub>2</sub> at microwave frequencies are among the lowest of all materials.<sup>5</sup>

MgF<sub>2</sub> has been used as a low refractive index material together with a higher refractive index material such as TiO<sub>2</sub>,<sup>6</sup> Sc<sub>2</sub>O<sub>3</sub>,<sup>7</sup> CeO<sub>2</sub>,<sup>8</sup> Al<sub>2</sub>O<sub>3</sub>,<sup>9,10</sup> or LaF<sub>3</sub><sup>11–14</sup> in optical multilayer structures. These multilayers have been used for a variety of optical applications, *e.g.* as highly radiation resistant high-reflecting coatings for UV lasers. MgF<sub>2</sub> thin films have also been applied in multilayers with conducting materials, *e.g.* with Ag<sup>15–18</sup> for flat panel displays and electromagnetic shielding, and with indium tin oxide (ITO) for solar cells.<sup>19</sup> MgF<sub>2</sub> film has also been used as a buffer layer for Pd in hydrogen sensors.<sup>20</sup>

MgF<sub>2</sub> is also widely used for enhancing the reflectance of aluminium mirrors in the vacuum UV region.<sup>21–26</sup> It is well known that aluminium oxidizes easily. To avoid the oxidation, aluminium has to be covered with a protective film. However, the cover layer can decrease dramatically the reflectance of Al, especially in the deep UV range. MgF<sub>2</sub> film would be an ideal solution to this, because MgF<sub>2</sub> is UV transparent with a low absorption coefficient. MgF<sub>2</sub>-protected aluminium films have been used in free-electron lasers, spectroscopy, and astrophysics.<sup>27</sup> Multilayer coatings of SiC, B<sub>4</sub>C/MgF<sub>2</sub> on Al were reported to have a high reflectance in the deep UV spectral range from 121.6 nm even down to 50 nm.<sup>28</sup>

Mainly physical vapor deposition (PVD) methods have been applied for fabricating MgF<sub>2</sub> thin films, *e.g.* thermal evaporation,<sup>27–35</sup> electron beam evaporation (EBE),<sup>4,12,21,36–38</sup> molecular beam deposition (MBD),<sup>33</sup> ion beam sputtering (IBS),<sup>31,37,39</sup> RF-magnetron sputtering,<sup>40</sup> ion beam assisted deposition (IBAD),<sup>41</sup> and plasma ion assisted deposition (PIAD).<sup>18,38,42</sup> The main limitation of evaporated MgF<sub>2</sub> films has been that they are porous with low packing densities.<sup>21</sup> The film structure is columnar and the intercolumnar voids take up water vapor. The result is an optically unstable layer with properties that are dependent on the degree of water absorption. However, the properties of MgF<sub>2</sub> films may be

<sup>a</sup>University of Helsinki, Department of Chemistry, P.O.Box 55, FIN-00014 University of Helsinki, Finland. E-mail: Tero.Pilvi@Helsinki.fi; Fax: +358 9 191 50198; Tel: +358 9 191 50219

<sup>b</sup>Accelerator Laboratory, P.O.Box 43, FIN-00014 University of Helsinki, Finland

<sup>c</sup>Friedrich-Schiller-University, Institute of Applied Physics, Max-Wien-Platz 1, 07743, Jena, Germany

<sup>d</sup>University Ulm, Central Facility of Electron Microscopy, Electron Microscopy Group of Materials Science, Albert Einstein Allee 11, D-89069, Ulm, Germany

<sup>e</sup>Fraunhofer Institute for Applied Optics and Precision Engineering, Albert-Einstein-Str. 7, 07745, Jena, Germany

<sup>†</sup> Present address: IMEC, Kapeldreef 75, 3001 Leuven, Belgium.

improved by Ar<sup>+</sup> ion bombardment: the transmittance is increased due to both a cleaning effect and a densification of the film structure.<sup>43</sup> The last effect could be a change from low packing densities to dense layers. Thermal annealing can also improve transmittance,<sup>43</sup> but annealing was reported to increase the amount of MgO in MgF<sub>2</sub> films.<sup>42</sup> Another problem in PVD methods is how to control the exact thickness of MgF<sub>2</sub> layers in multilayers.<sup>8</sup>

Chemical vapor deposition (CVD) of fluoride thin films has not been adopted widely so far due to difficulties in handling the fluorine precursors, namely hazardous HF or F<sub>2</sub> gas.<sup>44</sup> A few CVD processes have been reported for depositing MgF<sub>2</sub> films,<sup>44–47</sup> but the films suffer from low quality. Atomic layer deposition (ALD) belongs to the CVD methods and is becoming increasingly popular especially in microelectronic applications.<sup>48</sup> Controlling the layer thickness is very easy in ALD because the film is grown through alternate saturative surface reactions. Other benefits of ALD, besides the precise thickness accuracy, are uniformity, excellent step coverage, and high reproducibility.<sup>49</sup> ALD would be an ideal solution to, e.g. optical multilayers, where exact thickness and uniformity of layers are essential.

Deposition of fluoride thin films with ALD has been difficult, mainly because of a lack of a good fluorine precursor. In the first fluoride ALD studies HF, obtained by thermally decomposing NH<sub>4</sub>F, was used to deposit CaF<sub>2</sub>, ZnF<sub>2</sub>, and SrF<sub>2</sub>.<sup>50</sup> However, HF is an aggressive chemical which for example etches glass and is therefore not ideal for ALD. Recently we successfully used TiF<sub>4</sub> as a novel fluoride precursor for depositing CaF<sub>2</sub> thin films.<sup>51</sup> TiF<sub>4</sub> is a solid at room temperature and can thus be safely handled and removed from the reactor exhaust gases. In this paper, similar chemistry is studied for MgF<sub>2</sub> films. The metal precursor is Mg(thd)<sub>2</sub> (thd = bis(2,2,6,6-tetramethyl-3,5-heptanedionato) = C<sub>11</sub>H<sub>19</sub>O<sub>2</sub>) which has been used earlier in ALD<sup>52,53</sup> and CVD<sup>54</sup> of MgO.

## Experimental

### Synthesis and characterization of Mg(thd)<sub>2</sub>

Mg(thd)<sub>2</sub> was synthesized using two different methods. <sup>1</sup>H and <sup>13</sup>C NMR spectra were recorded in a Varian Gemini 2000 instrument at ambient temperature. Chemical shifts were referenced to SiMe<sub>4</sub> and are given in ppm. The mass spectrum was recorded with a JEOL JMS-SX102 operating in electron impact mode (70 eV) using a direct insertion probe and sublimation temperature range of 50–200 °C.

**Method 1.** All manipulations were done under exclusion of air and moisture using Schlenk techniques. Toluene was dried over 4 Å molecular sieves and deoxygenated with argon. 25.6 ml 1 M MgBu<sub>2</sub> solution in heptane (Aldrich) was dissolved in 50 ml dry toluene. During stirring 9.43 g Hthd was added to this solution. After stirring for 15 minutes solvents were evaporated under vacuum. The residue was dried under vacuum for 2 hours. The product was a clear or white glasslike material. Yield: 9.72 g (97.2%). Mp 122–126 °C. <sup>1</sup>H NMR (CDCl<sub>3</sub>) δ 1.09 (36H, m, CH<sub>3</sub>), 5.65 (2H, s, CH). <sup>13</sup>C{<sup>1</sup>H} NMR 28.27 (CH<sub>3</sub>), 28.42 (CH<sub>3</sub>), 28.83 (CH<sub>3</sub>), 40.96 (C(CH<sub>3</sub>)), 91.80 (CH), 201.43 (CO). MS (EI, 70 eV) *m/z* 780

[Mg<sub>2</sub>(thd)<sub>4</sub>]<sup>+</sup>, 597 [Mg<sub>2</sub>(thd)<sub>3</sub>]<sup>+</sup>, 390 [Mg(thd)<sub>2</sub>]<sup>+</sup>, 375 [Mg(thd)<sub>2</sub> – Me]<sup>+</sup>, 333 [Mg(thd)<sub>2</sub> – *t*Bu]<sup>+</sup>, 207 [Mg(thd)]<sup>+</sup>.

**Method 2.** Synthesis was done using the method of Schwarberg *et al.*<sup>55</sup> where Na(thd) and MgSO<sub>4</sub> are reacted in EtOH–H<sub>2</sub>O solution. After synthesis, the crude product was dried under vacuum and purified by sublimation at approximately 120 °C, 0.2 mbar. Sublimation resulted in a clear or white glasslike material. The yield after sublimation was 40–71%. The analysis results were identical with those observed for the product from method 1 and also with results reported earlier for structurally characterized Mg<sub>2</sub>(thd)<sub>4</sub>.<sup>52</sup>

### Film deposition

The films were grown in a hot-wall flow-type F120 ALD reactor (ASM-Microchemistry Ltd., Helsinki, Finland). All films were deposited at a temperature range of 250–400 °C. The pressure in the reactor was about 10 mbar. MgF<sub>2</sub> thin films were deposited mainly on 5 × 5 cm<sup>2</sup> Si(100) and Si(111) with native SiO<sub>2</sub>. Other substrates were 5 × 5 cm<sup>2</sup> borosilicate glass, ITO film on glass, and 2.5 × 5 cm<sup>2</sup> quartz. Mg(thd)<sub>2</sub> was evaporated from an open glass crucible at 125 °C and TiF<sub>4</sub> (Strem Chemicals Inc.) at 145 °C inside the reactor. Mg(thd)<sub>2</sub> and TiF<sub>4</sub> pulse times varied from 0.5 to 4 s and 0.5 to 2 s, respectively. Nitrogen (>99.999% NITROX UHPN 3000 nitrogen generator) was used as carrier and purging gas. Nitrogen purges (0.5–1.0 s) were used after both precursor pulses to separate the precursors in the gas phase and to remove the excess reactants and gaseous reaction byproducts.

### Film characterization

Adhesion of the films was tested with a tape test. Thicknesses and refractive indices of the MgF<sub>2</sub> thin films were determined from optical reflection or transmission spectra obtained with a Hitachi U2000 spectrophotometer in the wavelength range of 190–1100 nm. A fitting program developed and described by Ylilammi and Ranta-aho<sup>56</sup> was used in analyzing the spectra. The error in the film thickness measurements was estimated to be ±5%. Other transmission spectra were obtained with a Lambda850 spectrometer in the wavelength range of 140–800 nm.

Film thicknesses, densities and crystalline structures were evaluated from X-ray reflection (XRR) and grazing incidence X-ray diffraction (GI-XRD) patterns measured with a PANalytical X'pert Pro MPD X-ray diffractometer. Film thicknesses were analyzed by XRR only for the thinnest films up to 38 nm; otherwise, they were measured by UV-vis spectroscopy.

Film crystalline structure and morphology were studied with transmission electron microscopy (TEM) and scanning electron microscopy (SEM). For TEM studies a JEOL JEM 3010 was used operated at 300 kV, with a point-to-point resolution of 0.21 nm. TEM cross-sectional sample preparation was carried out using standard techniques including mechanical polishing and Ar ion thinning. For SEM studies a Hitachi S4800 FESEM instrument was used. Before the SEM analysis, the samples were sputter-coated with a thin Pd–Pt alloy (Cressington 208HR Sputter Coater).

Film surface roughness was also studied with atomic force microscopy (AFM) using a Veeco Instrument Nanoscope V. Samples were measured in tapping mode in air using a phosphorus doped silicon probe (RTESP) delivered by Veeco Instrument with a scanning frequency of 0.5 Hz. Several scans were performed from different parts of the samples to check the uniformity of the surface. Roughness values were calculated as root-mean-square values ( $R_q$ ) from the final images that were measured from a scanning area of  $2 \times 2 \mu\text{m}^2$ . No image processing except flattening was performed.

Composition and impurity levels of the films were analyzed by time-of-flight elastic recoil detection analysis (TOF-ERDA) using a 24 MeV  $^{127}\text{I}^{5+}$  projectile ion beam.<sup>57</sup>

Electrical properties of the films were measured from Al/MgF<sub>2</sub>/ITO capacitor structures on glass. These were prepared by depositing approximately 100 nm thick Al top electrode dots with an area of  $2.04 \times 10^{-7} \text{m}^2$  on the top of the MgF<sub>2</sub> film by e-beam evaporation through a shadow mask. Permittivities of the films were measured using a HP 4284A precision LCR-meter at 10 kHz. A Keithley 2400 SourceMeter was used to measure leakage current densities. All electrical properties were measured at room temperature.

## Results and discussion

### Precursor synthesis

For comparison two different methods were employed to synthesize Mg(thd)<sub>2</sub>: 1) reaction between MgBu<sub>2</sub> and Hthd in toluene, and 2) the method of Schwarberg *et al.*<sup>55</sup> where Na(thd) and MgSO<sub>4</sub> are reacted in EtOH–H<sub>2</sub>O solution. In method 2 the product needs to be isolated and purified by sublimation while method 1 conducted under dry toluene produces the volatile byproduct butane and gives pure Mg(thd)<sub>2</sub> straight from the synthesis. Analysis and thin film growth experiments proved that the methods produce identical Mg(thd)<sub>2</sub>. The yield of method 2 after sublimation was always less than 71% while method 1 gave yields close to 100%. MgBu<sub>2</sub> used in method 1 is readily available as a solution from chemical suppliers. To conclude, method 1 is preferred because it is a fast and very efficient room temperature method with good yields.

### Film growth

MgF<sub>2</sub> growth characteristics were studied by depositing films on silicon between 250 and 400 °C. Self-limitation of the ALD process was studied at 250 °C by varying the Mg(thd)<sub>2</sub> pulse length (Fig. 1). In these experiments both TiF<sub>4</sub> pulse and purge times were 1.0 s. A growth rate of about 1.6 Å cycle<sup>-1</sup> was achieved after 3.0 s Mg(thd)<sub>2</sub> pulse. At first, this 3.0 s pulse time seems long compared to many other ALD processes in the same reactor, but it is similar to the CaF<sub>2</sub> ALD process, where the Ca(thd)<sub>2</sub> pulse length needed for saturation was 2.5 s.<sup>51</sup> As seen in Fig. 1 the growth rate does not fully saturate with reasonable pulse lengths. Mg(thd)<sub>2</sub> was reported not to decompose at 250 °C,<sup>53</sup> so there seems to be another reason for the incomplete saturation, *e.g.*, a slow half-reaction. It is also possible that TiF<sub>x</sub> surface species catalyze Mg(thd)<sub>2</sub> decomposition in some way.

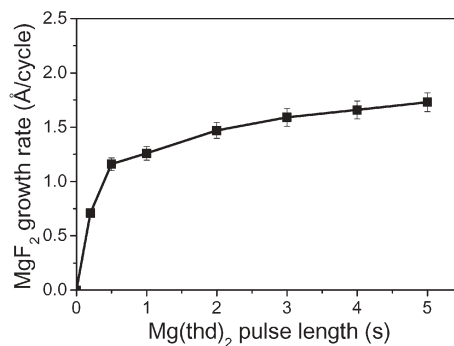


**Fig. 1** Growth rate of MgF<sub>2</sub> films on silicon as a function of Mg(thd)<sub>2</sub> pulse length at 250 °C. TiF<sub>4</sub> pulse and purge times were 1.0 s.

A theoretical maximum growth rate in ALD is one monolayer cycle<sup>-1</sup> but this high rate is rarely observed because of steric hindrances of precursors.<sup>58</sup> The monolayer thickness of MgF<sub>2</sub> is 1.53 Å as calculated from the crystal structure and lattice parameters (tetragonal MgF<sub>2</sub>  $a = 4.62 \text{Å}$  and  $c = 3.05 \text{Å}$ ).<sup>3</sup> The obtained growth rate of 1.6 Å cycle<sup>-1</sup> equals about one monolayer of MgF<sub>2</sub> but is uncommonly high for a thermal ALD process.<sup>58</sup> One explanation for this high growth rate can be found from the unique growth mechanism. As a net reaction the following ligand exchange is suggested:



The reaction of Mg(thd)<sub>2</sub> and TiF<sub>4</sub> results in a solid MgF<sub>2</sub> deposit, volatile Ti(thd)<sub>4</sub> and possibly other volatile byproducts such as TiF<sub>x</sub>(thd)<sub>4-x</sub>. In ALD the overall reaction is divided into two steps occurring during the two pulses. Similar to our previous CaF<sub>2</sub> ALD process,<sup>51</sup> the mechanism shown in Fig. 2 is suggested. The reaction scheme starts with a Mg(thd)<sub>2</sub> pulse (Fig. 2a). The preceding TiF<sub>4</sub> pulse has left TiF<sub>x</sub> adsorbed on the surface of previously deposited MgF<sub>2</sub>. The incoming Mg(thd)<sub>2</sub> first reacts with TiF<sub>x</sub> forming solid MgF<sub>2</sub> and volatile Ti(thd)<sub>4</sub>. After Mg(thd)<sub>2</sub> has consumed all TiF<sub>x</sub> on the surface, Mg(thd)<sub>2</sub> still adsorbs on top of the freshly formed solid MgF<sub>2</sub> and the surface becomes covered by adsorbed Mg(thd)<sub>x</sub>. Then during the TiF<sub>4</sub> pulse (Fig. 2b), TiF<sub>4</sub> reacts

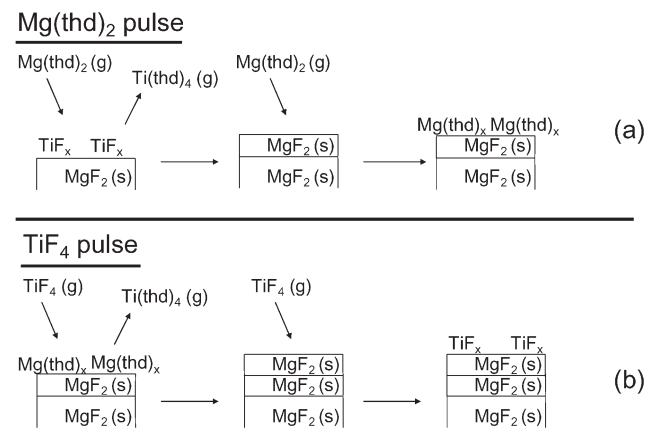


**Fig. 2** Suggested reaction mechanism in MgF<sub>2</sub> ALD during (a) Mg(thd)<sub>2</sub> pulse, and (b) TiF<sub>4</sub> pulse. N<sub>2</sub> purges are always applied after each precursor pulses. MgF<sub>2</sub> is formed in both half reactions.

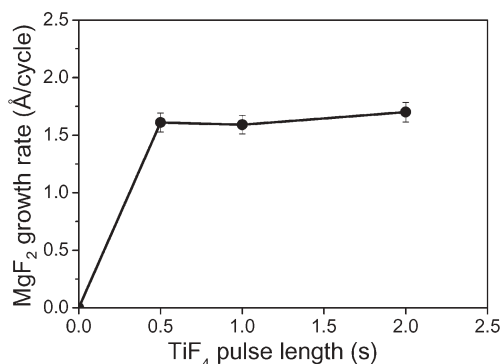


**Fig. 3** Growth rate of MgF<sub>2</sub> films on silicon as a function of TiF<sub>4</sub> pulse length at 250 °C. Mg(thd)<sub>2</sub> pulse time was 3.0 s and purge time 0.5 s.

with Mg(thd)<sub>x</sub>, and volatile Ti(thd)<sub>4</sub> and solid MgF<sub>2</sub> are formed. Once TiF<sub>4</sub> has reacted with all Mg(thd)<sub>x</sub> on the surface, TiF<sub>x</sub> adsorbates are formed on top of the deposited solid MgF<sub>2</sub>. This leads back to the start of the scheme (Fig. 2a). In summary, MgF<sub>2</sub> is formed in both half reactions during one ALD cycle. Such a mechanism could explain the high 1.6 Å cycle<sup>-1</sup> growth rate of the MgF<sub>2</sub> film. An interesting question is how completely Ti atoms and the thd ligands can be removed from the film. This is related directly to the impurity levels and the transparency of the film, which we will see later on.

Fig. 3 depicts the MgF<sub>2</sub> growth rate as a function of the TiF<sub>4</sub> pulse length at 250 °C. The Mg(thd)<sub>2</sub> pulse length was 3.0 s. Saturation of the growth rate was achieved already after 0.5 s pulse time of the anion source TiF<sub>4</sub>. Upon doubling the purge time from 0.5 s to 1.0 s, the growth rate decreased only slightly from 1.6 to 1.5 Å cycle<sup>-1</sup>, and therefore 0.5 s purge times were considered sufficient.

Thicknesses of the MgF<sub>2</sub> films are illustrated in Fig. 4 as a function of the number of deposition cycles. MgF<sub>2</sub> film thickness depends almost linearly on the number of deposition cycles, which is characteristic for ALD. Linear growth rate was about 1.6 Å cycle<sup>-1</sup>.

The dependence of the growth rate on the deposition temperature is shown in Fig. 5. The maximum growth rate of 1.6 Å cycle<sup>-1</sup> was achieved at 250 °C. The growth rate decreased quite rapidly with increasing deposition temperature. Anyhow, the growth rate was still 1.3 Å cycle<sup>-1</sup> at 300 °C, but 0.8 Å cycle<sup>-1</sup> at 350 °C, and 0.7 Å cycle<sup>-1</sup> at 400 °C.

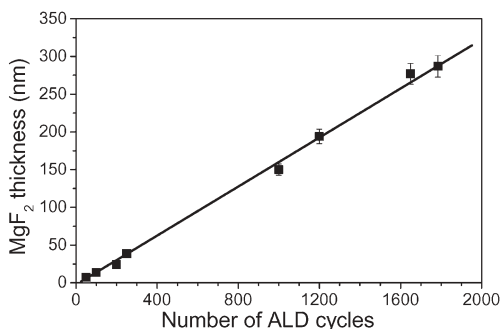


**Fig. 4** Film thickness vs. number of deposition ALD cycles at 250 °C.

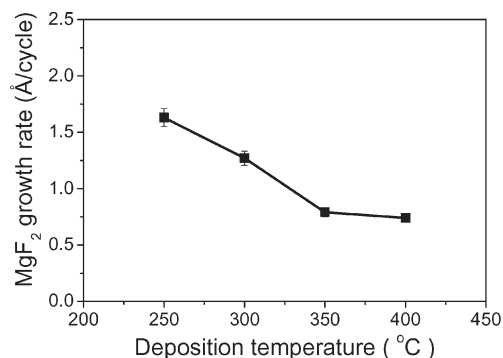


**Fig. 5** Growth rate of MgF<sub>2</sub> films on silicon as a function of deposition temperature. Mg(thd)<sub>2</sub> pulse length was 3.0 s whereas TiF<sub>4</sub> pulse and purge times were 0.5 s.

Decreasing growth rate with increasing deposition temperature was also observed earlier in the CaF<sub>2</sub> ALD processes from Ca(thd)<sub>2</sub> + TiF<sub>4</sub>,<sup>51</sup> and Ca(thd)<sub>2</sub> + HF.<sup>50</sup>

### Film properties

All the films passed the tape adhesion test. The films were polycrystalline magnesium fluoride as determined by GI-XRD. Fig. 6 shows the diffraction patterns obtained from MgF<sub>2</sub> thin films grown at 250–400 °C. The film deposited at 250 °C showed (110), (210), (211), and (220) reflections. In addition, the film deposited at 400 °C showed (101), (111) and (002) reflections. Crystallinity of the films increased with the deposition temperature as expected. These results are in good agreement with Atanassov *et al.*<sup>38</sup> who reported that crystallization of MgF<sub>2</sub> thin films begins at temperatures above 250 °C.

Cross-sectional TEM images of a MgF<sub>2</sub> thin film deposited at 250 °C (Fig. 7) support the XRD results on crystallization of the film already at the lowest deposition temperature studied. The dark field image with the diffraction pattern inserted shows the columnar structure of the layer (Fig. 7a) and the columns consisting of grains with a range of preferred orientations (arcs in the diffraction pattern). In the diffraction pattern sharp reflections correspond to the Si substrate and arcs to the MgF<sub>2</sub> layer. A high resolution TEM image from the interface region (Fig. 7b) reveals random distribution of the

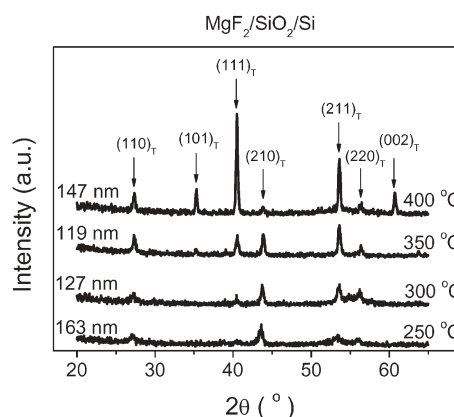


**Fig. 6** GI-XRD patterns of MgF<sub>2</sub> thin films grown on Si(100) at temperatures between 250 and 400 °C.

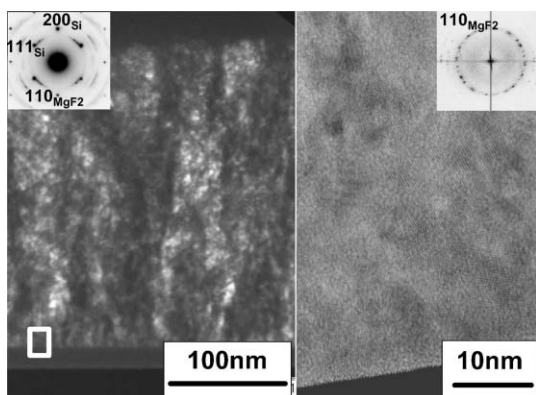


**Fig. 7** Cross-sectional dark field TEM image (a) and high resolution TEM image from the interface region (b) (marked by white rectangle in (a)) of a  $\text{MgF}_2$  thin film deposited at 250 °C. The insert in (a) is an electron diffraction pattern while that in (b) is a FFT pattern of the image.

small crystalline grains in the initial stage of the growth (see the fast Fourier transform (FFT) inserted in Fig. 7b).

The morphology of the films was analyzed from the SEM images (Fig. 8 and 9). Only small grains were formed at 250 °C (Fig. 8a) but larger grains were grown at higher temperatures (Fig. 8b, c, and d). Cross-sectional SEM images of  $\text{MgF}_2$  films on silicon are shown in Fig. 9. A columnar structure can be seen in films deposited at 250 °C and 350 °C. The columnar structure is clearer in the film deposited at 350 °C; obviously this film is also rougher than the film deposited at 250 °C. Evaporated  $\text{MgF}_2$  films were reported to have columnar structures on silicon<sup>59</sup> and amorphous substrates.<sup>60</sup> In contrast, our earlier experiments showed that ALD  $\text{CaF}_2$  grew granularly on silicon at 300 °C.<sup>51</sup>

Densities of the films deposited at 250–400 °C were 2.4–2.7  $\text{g cm}^{-3}$  as measured by XRR. The density increased with growth temperature, and was in good agreement with the values reported for evaporated  $\text{MgF}_2$  films,<sup>61</sup> but remained lower than the tetragonal  $\text{MgF}_2$  bulk density of 3.15  $\text{g cm}^{-3}$ .

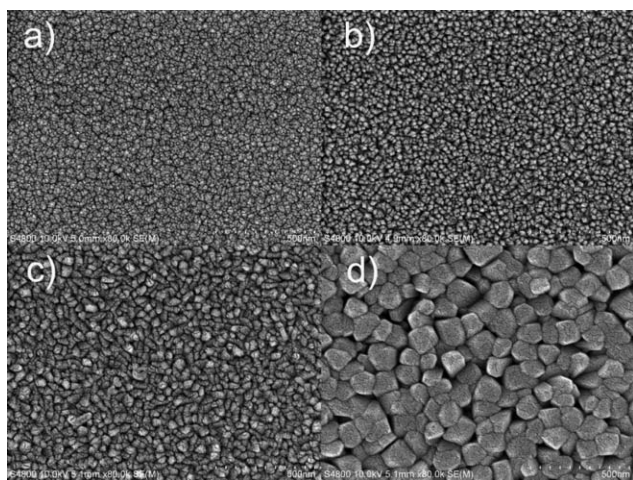


**Fig. 8** SEM images of  $\text{MgF}_2$  thin films on silicon. Deposition temperatures and thicknesses of the films were (a) 250 °C, 163 nm, (b) 300 °C, 127 nm, (c) 350 °C, 119 nm, and (d) 400 °C, 147 nm.

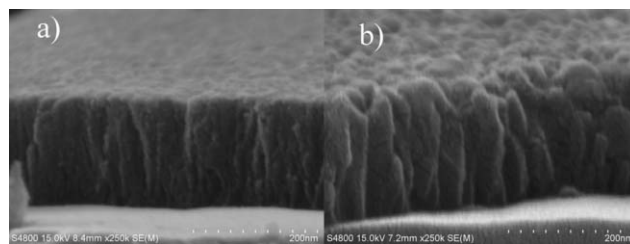


**Fig. 9** Cross-section SEM images of  $\text{MgF}_2/\text{SiO}_2/\text{Si}$ . Deposition temperatures and thicknesses of the films were (a) 250 °C, 170 nm, and (b) 350 °C, 200 nm.

Due to impurities in the films, the density can be lower than the bulk value. Roughnesses of the films deposited at 250 °C were 0.8–0.9 nm for 8.0, 14.6 and 24.2 nm thick  $\text{MgF}_2$  films as measured by XRR.

The surface roughness of  $\text{MgF}_2$  films on silicon was also measured by AFM (Table 1) from thicker films. As expected, the roughness (nm) increased with increasing deposition temperature: 3.3 at 250 °C, 5.8 at 300 °C, 6.3 at 350 °C, and remarkably 23.0 at 400 °C. This increased film roughness can also be seen in Fig. 8 and 9. The increased roughness and consequent light scattering make the films grown at the highest deposition temperature poor candidate for optical applications.

Film compositions were determined by TOF-ERDA (Table 2). UV optics materials like  $\text{MgF}_2$  must have very low levels of transition metal impurities or other elements that absorb in the UV range. It was reported that the impurity contents must be below 0.5% and in some cases below 0.1% by weight.<sup>1</sup> The reported contents (Table 2) are averages found in the bulk of the films excluding the surface and interface regions. The films were fluorine rich at lower temperatures: the F : Mg ratio was 2.2 at 250 °C, 2.1 at 300 °C, and 2.0 at 350–400 °C. The total impurity contents (at.%) in the films decreased with increasing deposition temperature: 19.6 at 250 °C, 5.6 at 300 °C, 0.6 at 350 °C, and only 0.3 at 400 °C. It is unfortunate, however, that the highest purity is combined with

**Table 1** Surface roughness of  $\text{MgF}_2$  films on Si as measured by AFM

Growth temperature/°C	Thickness/nm	Roughness/nm
250	163	3.3
300	127	5.8
350	102	6.3
400	147	23.0

**Table 2** Composition (at.%) of  $\text{MgF}_2$  thin films deposited at different temperatures as measured by TOF-ERDA

	250 °C	300 °C	350 °C	400 °C
F	55.5	64.0	66.7	66.2
Mg	24.9	30.7	32.7	33.5
O	4.3	1.0	0.3	0.1
Ti	2.8	1.4	0.2	<0.1
C	4.1	1.0	<0.1	0.1
N	<0.1	<0.1	<0.1	<0.1
H	8.4	1.9	<0.1	<0.1
B	<0.1	<0.1	0	<0.1
F : Mg	2.2	2.1	2.0	2.0

the highest roughness (Table 1). These low impurity levels indicate that the suggested ligand exchange reaction (1) is efficient and proceeds close to completion. Boron impurities were also detected, and they most likely originate from the borosilicate glass substrate. The impurity contents are lower than detected in  $\text{MgF}_2$  films deposited by evaporation and ion beam sputtering methods, which both contained in total 2.0 at.% C and O.<sup>39</sup>

Refractive indices were evaluated from reflection spectra because most of the films were deposited onto silicon. Low refractive indices were obtained and they decreased as a function of deposition temperature: 1.42 at 250 °C, 1.38 at 300 °C, 1.37 at 350 °C, and 1.34 at 400 °C ( $\lambda = 580$  nm). The bulk refractive index is 1.378 ( $\lambda = 589$  nm) for tetragonal  $\text{MgF}_2$ .<sup>3</sup> The 250 °C film has a refractive index higher than the bulk which may be due to the impurities in the films, titanium in particular. The low refractive index of the film deposited at 400 °C is typically a result of the porous microstructure,<sup>34</sup> which is also seen in Fig. 8d, where the voids left between the grains increase the porosity despite the increased grain size.

Fig. 10 shows transmission spectra of  $\text{MgF}_2$  films grown on quartz at 300 °C (dash and dot line) and 350 °C (dash line), and a reference spectrum of bare quartz (solid line) in the wavelength ranges of a) 140–230 nm, and b) 175–800 nm. Both samples have higher transmission than the quartz substrate in the high wavelength range of 500–800 nm (Fig. 10b). The transmission drops below that of the quartz substrate at about

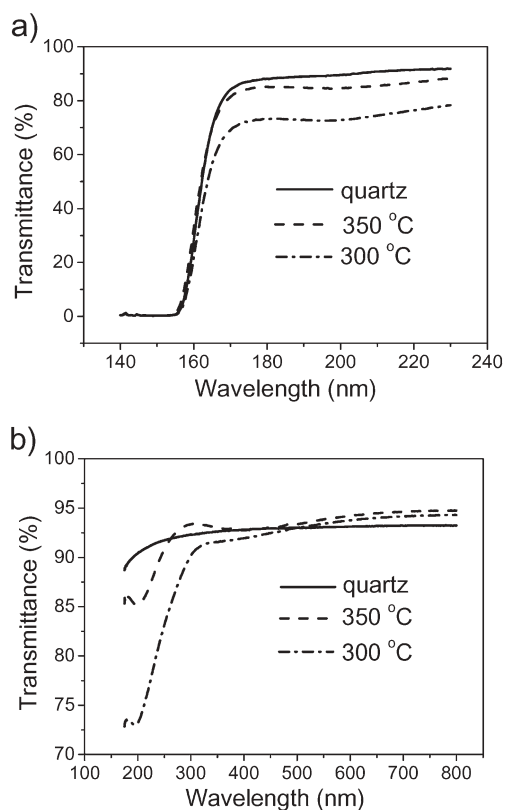


**Fig. 10** Transmission spectra of a quartz substrate and  $\text{MgF}_2$  films on quartz in wavelength range of (a) 140–230 nm, and (b) 175–800 nm. Thickness of the  $\text{MgF}_2$  film deposited at 300 °C was 146 nm, and at 350 °C it was 155 nm.

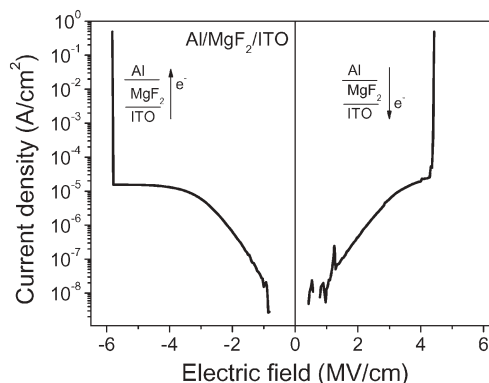


**Fig. 11** Leakage current density vs. electric field curves of Al/ $\text{MgF}_2$ /ITO capacitors. Thickness of the  $\text{MgF}_2$  film grown at 250 °C was about 140 nm.

500 nm for the sample deposited at 300 °C. However, the transmission of the sample deposited at 350 °C drops below the quartz line only at 260 nm. Transmittance is still 92% at 260 nm and 86% at 180 nm and remains at this level down to the absorption edge of the quartz substrate. The main reason for the better transmittance of the 350 °C sample is apparently the lower impurity content: 0.6 vs. 5.6 at.% (Table 2). Nevertheless, although the impurity levels in the films were low according to TOF-ERDA, they are not low enough for really high transmission in vacuum UV. The  $\text{MgF}_2$  film deposited on borosilicate glass at 250 °C is hydrolytically stable, because the transmittance stayed the same in the wavelength range of 370–1100 nm after 12 months storage in air (data not shown).

Electrical properties were measured for a *ca.* 140 nm thick  $\text{MgF}_2$  film in Al/ $\text{MgF}_2$ /ITO capacitor structures. The average permittivity obtained for the  $\text{MgF}_2$  film grown at 250 °C was 4.9 at 10 kHz which is close to the reported value of 5.45 at 1 MHz.<sup>5</sup> The leakage current density of the film vs. electric field is shown in Fig. 11. Catastrophic breakdown occurred at electric fields of  $-5.8$  and  $+4.4$   $\text{MV cm}^{-1}$ . These are significantly better than what was reported earlier,  $0.2$   $\text{MV cm}^{-1}$  for a 292 nm thick  $\text{MgF}_2$  film deposited by thermal evaporation,<sup>62</sup> and  $-0.3$  and  $+0.4$   $\text{MV cm}^{-1}$  for 200 nm ALD  $\text{CaF}_2$ .<sup>51</sup> Before the breakdown, the leakage current density was below  $10^{-5}$   $\text{A cm}^{-2}$ .

## Conclusions

$\text{MgF}_2$  thin films were deposited for the first time by ALD at 250–400 °C.  $\text{Mg}(\text{thd})_2$  and  $\text{TiF}_4$  were used as precursors. The films were polycrystalline and grew in a columnar fashion on silicon. The film densities were  $2.4$ – $2.7$   $\text{g cm}^{-3}$ , increasing with the deposition temperature. Films with ideal stoichiometry and low impurity levels were obtained at 350–400 °C. Unfortunately, the highest purity achieved at 400 °C is accompanied by increased surface roughness. Refractive indices were 1.34–1.42. Transmittances of 93% at 300 nm, and 86% at 180 nm were obtained in the UV range with a film deposited at 350 °C. Permittivity of the film deposited at 250 °C was 4.9, and breakdown occurred at electric field values of  $-5.8$  and  $+4.4$   $\text{MV cm}^{-1}$ , in the Al/ $\text{MgF}_2$ /ITO capacitors. In

summary, the results clearly demonstrate that ALD is a suitable method for deposition of quality MgF<sub>2</sub> thin films.

## References

- 1 UV Coatings: Materials and Applications, *CERAC Coat. Mater. News*, 2002, **12**, 1–4 (<http://www.cerac.com/pubs/CMNarchives.htm>).
- 2 M. Scrocco, *Phys. Rev. B*, 1986, **33**, 7228–7231.
- 3 Physical Constants of Organic Compounds, in *CRC Handbook of Chemistry and Physics*, Internet Version 2007, 87th edn, ed. D. R. Lide, Taylor and Francis, Boca Raton, FL, 2007.
- 4 J. Heber, C. Muehlig, W. Triebel, N. Danz, R. Thielsch and N. Kaiser, *Appl. Phys. A*, 2003, **76**, 123–128.
- 5 M. V. Jacob, J. Krupka, J. Mazierska and G. S. Woods, *Mater. Sci. Eng., A*, 2006, **427**, 175–180.
- 6 Y. J. Lee, J. H. Lee, Y. Y. Lee, Y. H. Kang, Y. S. Kim, S. N. Kwon and K. Jeong, *Opt. Commun.*, 2001, **190**, 211–220.
- 7 S. Tamura, S. Kimura, Y. Sato, S. Motokoshi, H. Yoshida and K. Yoshida, *Jpn. J. Appl. Phys.*, 1990, **29**, 1960–1962.
- 8 S. E. Lee, S. W. Choi and J. Yi, *Thin Solid Films*, 2000, **376**, 208–213.
- 9 S. Shuzhen, S. Jianda, L. Chunyan, Y. Kui, F. Zhengxiu and C. Lei, *Appl. Surf. Sci.*, 2005, **249**, 157–161.
- 10 M. Zhan, W. Gao, T. Tan, H. He, J. Shao and Z. Fan, *Vacuum*, 2005, **79**, 90–93.
- 11 S. Guenster, D. Ristau, A. Gatto, N. Kaiser, M. Trovo and F. Sarto, *Proceedings of the 26th International Free Electron Conference FEL*, ed. R. Bakker, L. Giannessi, M. Marsi and R. Walker, Comitato Conferenze Elettra, Trieste, Italy, 2004, pp. 233–236.
- 12 E. Welsch, K. Ettrich, H. Blaschke and N. Kaiser, *Appl. Surf. Sci.*, 1996, **96–98**, 393–398.
- 13 Z. Czigan, M. Adamik and N. Kaiser, *Thin Solid Films*, 1998, **312**, 176–181.
- 14 S. Jakobs, A. Duparre and H. Truckenbrodt, *Int. J. Machine Tools Manuf.*, 1998, **38**, 733–739.
- 15 M. J. Bloemer and M. Scalora, *Appl. Phys. Lett.*, 1998, **72**, 1676.
- 16 M. Scalora, M. J. Bloemer, A. S. Pethel, J. P. Dowling, C. M. Bowden and A. S. Manka, *J. Appl. Phys.*, 1998, **83**, 2377.
- 17 X. Xu, Z. Tang, J. Shao and Z. Fan, *Appl. Surf. Sci.*, 2005, **245**, 11–15.
- 18 J. K. Fu, G. Atanassov, Y. S. Dai, F. H. Tan and Z. Q. Mo, *J. Non-Cryst. Solids*, 1997, **218**, 403–410.
- 19 E. J. Simburger, J. H. Matsumoto, T. W. Giants, A. Garcia, III, S. Liu, S. P. Rawal, A. R. Perry, C. H. Marshall, J. K. Lin and S. E. Scarborough, *Mater. Sci. Eng., B*, 2005, **116**, 265–272.
- 20 A. Chtanov and M. Gal, *Sens. Actuators, B*, 2001, **79**, 196–199.
- 21 P. J. Martin, W. G. Saintry, R. P. Nettlefield, D. R. McKenzie, D. J. H. Cockayne, S. H. Sie, O. R. Wood and H. G. Craighead, *Appl. Opt.*, 1987, **26**, 1235–1239.
- 22 P. Maier-Komor, J. Friese, R. Gernhauser, J. Homolka, R. Krucken and S. Winkler, *Nucl. Instrum. Methods Phys. Res., Sect. A*, 2004, **521**, 35–42.
- 23 N. L. Thomas and J. D. Wolfe, *Proc. SPIE-Int. Soc. Opt. Eng.*, 2000, **4003**, 312–323.
- 24 E. T. Hutcheson, G. Hass and J. T. Cox, *Appl. Opt.*, 1972, **11**, 2245.
- 25 W. R. Hunter, J. F. Osantowski and G. Hass, *Appl. Opt.*, 1971, **10**, 540.
- 26 L. R. Canfield, G. Hass and J. E. Waylonis, *Appl. Opt.*, 1966, **5**, 45–49.
- 27 M. Fernandez-Perea, J. A. Aznarez, J. Calvo-Angos, J. I. Larruquert and J. A. Mendez, *Thin Solid Films*, 2006, **497**, 249–253.
- 28 J. I. Larruquert and R. A. M. Keski-Kuha, *Appl. Opt.*, 1999, **38**, 1231–1236.
- 29 M. C. Larciprete, N. Savalli, T. Tenev, M. Scalora, G. Leahu, C. Sibilila, S. Baglio, K. Panajotov and M. Bertolotti, *Appl. Phys. B*, 2005, **81**, 245–249.
- 30 Q. Wang, W. Lei, X. Zhang, B. Wang, M. Liu, X. Zhou, Y. Di and X. Ma, *Appl. Surf. Sci.*, 2005, **239**, 458–463.
- 31 J. I. Larruquert and R. A. M. Keski-Kuha, *Opt. Commun.*, 2003, **215**, 93–99.
- 32 M. C. Larciprete, C. Sibilila, S. Paoloni, G. Leahu, R. Li Voti, M. Bertolotti, M. Scalora and K. Panajotov, *J. Appl. Phys.*, 2002, **92**, 2251–2255.
- 33 U. Kaiser, M. Adamik, G. Safran, P. B. Barna, S. Laux and W. Richter, *Thin Solid Films*, 1996, **280**, 5–15.
- 34 A. Zuber, N. Kaiser and J. L. Stehle, *Thin Solid Films*, 1995, **261**, 37–43.
- 35 V. Z. Rysanek, *Appl. Opt.*, 1965, **4**, 993–997.
- 36 S. Linden, M. Decker and M. Wegener, *Phys. Rev. Lett.*, 2006, **97**, 083902.
- 37 D. Ristau, S. Gunster, S. Bosch, A. Duparre, E. Masetti, J. Ferre-Borrull, G. Kiriakidis, F. Peiro, E. Quesnel and A. Tikhonravov, *Appl. Opt.*, 2002, **41**, 3196.
- 38 G. Atanassov, J. Turlo, J. K. Fu and Y. S. Dai, *Thin Solid Films*, 1999, **342**, 83–92.
- 39 D. Jacob, F. Peiro, E. Quesnel and D. Ristau, *Thin Solid Films*, 2000, **360**, 133–138.
- 40 K. Kawamata, T. Shouzu and N. Mitamura, *Vacuum*, 1998, **51**, 559–564.
- 41 S. Scaglione, D. Flori, I. Soymie and A. Piegari, *Thin Solid Films*, 1992, **214**, 188–193.
- 42 W. Seouk-Hoon and H. Chang Kwon, *Appl. Opt.*, 2006, **45**, 1447.
- 43 F. Perales, J. M. Herrero, D. Jaque and C. de las Heras, *Opt. Mater.*, 2007, **29**, 783–787.
- 44 S. Fujihara, M. Tada and T. Kimura, *Thin Solid Films*, 1997, **304**, 252–255.
- 45 T. Murata, H. Ishizawa, I. Motoyama and A. Tanaka, *J. Sol-Gel Sci. Technol.*, 2004, **322**, 161–165.
- 46 I. M. Thomas, *Appl. Opt.*, 1988, **27**, 3356.
- 47 P. H. Joosten, P. Heller, H. J. P. Nabben, H. A. M. van Hal, T. J. A. Popma and J. Haisma, *Appl. Opt.*, 1985, **24**, 2674.
- 48 M. Leskelä and M. Ritala, *Angew. Chem., Int. Ed.*, 2003, **42**, 5548–5554.
- 49 M. Ritala and M. Leskelä, *Handbook of Thin Film Materials*, Academic Press, San Diego, 2001, p. 103.
- 50 M. Ylilammi and T. Ranta-aho, *J. Electrochem. Soc.*, 1994, **141**, 1278–1284.
- 51 T. Pilvi, K. Arstila, M. Leskelä and M. Ritala, *Chem. Mater.*, 2007, **19**, 3387–3392.
- 52 T. Hatanpää, J. Ihanus, J. Kansikas, I. Mutikainen, M. Ritala and M. Leskelä, *Chem. Mater.*, 1999, **11**, 1846–1852.
- 53 M. Putkonen, L. Johansson, E. Rauhala and L. Niinistö, *J. Mater. Chem.*, 1999, **9**, 2449–2452.
- 54 B. S. Kwak, E. P. Boyd, K. Zhang, A. Erbil and B. Wilkins, *Appl. Phys. Lett.*, 1989, **54**, 2542–2544.
- 55 J. E. Schwarberg, R. E. Sievers and R. W. Moshier, *Anal. Chem.*, 1970, **42**, 1828–1830.
- 56 M. Ylilammi and T. Ranta-aho, *Thin Solid Films*, 1993, **232**, 56–62.
- 57 M. Putkonen, T. Sajavaara, L. Niinistö and J. Keinonen, *Anal. Bioanal. Chem.*, 2005, **382**, 1791–1799.
- 58 M. Ylilammi, *Thin Solid Films*, 1996, **279**, 124–130.
- 59 A. Duparre, C. Ruppe, K. A. Pischow, M. Adamik and P. B. Barna, *Thin Solid Films*, 1995, **261**, 70–75.
- 60 U. Kaiser, N. Kaiser, P. Weisbrodt, U. Mademann, E. Hacker and H. Muller, *Thin Solid Films*, 1992, **217**, 7–16.
- 61 A. Coban, E. E. Khawaja and S. M. A. Durrani, *Nucl. Instrum. Methods Phys. Res., Sect. B*, 2002, **194**, 171–176.
- 62 J. K. Ko, D. Y. Kim, J. H. Park, S. W. Choi, S. H. Park and J. Yi, *Thin Solid Films*, 2003, **427**, 259–265.